DES AND URANS OF A TURBULENT BOUNDARY LAYER ON A CONCAVE WALL

Joongcheol Paik, S Casey Jones, Fotis Sotiropoulos
School of Civil and Environmental Engineering
Georgia Institute of Technology
Atlanta, GA 30332-0355 USA

ABSTRACT

Coherent streamwise vortical structures inside the centrifugally unstable turbulent boundary layer on the concave (outer) wall of a 90 deg duct are simulated numerically using DES and URANS coupled with an instantaneous random forcing technique to generate inlet boundary conditions. The simulated vortical structures originate approximately halfway through the bend, span the entire concave wall, meander randomly in space, and exhibit intense low-frequency, unsteadiness. Our results show that these structures account for a significant percentage of the total Reynolds stresses inside the concave wall boundary layer but do not result in appreciable spanwise variations of the mean velocity field.

INTRODUCTION

Turbulence modeling strategies that resolve large-scale, unsteady, coherent structures in the flow have great promise in flows in which organized unsteadiness accounts for a significant percentage of the overall Reynolds stresses. For the most part, such models have been applied to external, massively separated flows (Squires et al. 2002), but their predictive capabilities in complex, internal flows have yet to be investigated.

In this work, we employ the detached-eddy simulation (DES) (Spalart et al. 1997) approach and various unsteady RANS (URANS) turbulence models to simulate the centrifugal instability of a turbulent boundary layer developing along a concave wall. Concave wall turbulence is important in many applications of engineering practice, but its underlying physics continue to be at the center of considerable controversy in the literature and to elude accurate prediction by standard steady RANS models (Patel and Sotiropoulos 1997). In spite of the controversy, however, there is now considerable numerical (Lund and Moin 1996) and experimental (Barlow and Johnston 1988) evidence to suggest that the well known dramatic increase of Reynolds-stresses inside a concave wall boundary layer is at least partly due to the presence of large-scale, low-frequency unsteady vortical structures in the flow. Therefore, such flows are, at least in principle, suitable for study with unsteady, statistical turbulence models.

We employ DES and URANS turbulence models to simulate the flow in the strongly curved, 90-deg, rectangular duct whose mean flow and turbulence statistics have been documented experimentally by Kim and Patel (1994). This flow is a standard test case in ERCOFTAC workshops and has also been studied in detail by Sotiropoulos and Ventikos (1998) who employed a variety of linear and non-linear, steady RANS turbulence models. This latter work showed that non-linear two-equation models that are valid all the way to the wall can capture the growth and evolution of the pressure-driven secondary motion along the inner (convex) wall of the bend with good accuracy. Sotiropoulos and Ventikos (1998) reported good agreement for the turbulence statistics near the convex wall of the bend, but their simulations failed to capture the measured (Kim and Patel 1994) dramatic increase of the Reynolds stresses inside the concave wall boundary layer, especially near the duct plane of symmetry. In this study we seek to: 1) explore whether large-scale, coherent vortices in the concave wall boundary layer of the Kim and Patel duct exist and can be predicted with unsteady statistical turbulence models; 2) elucidate the dynamics of these coherent structures with emphasis on their effect on the mean flow and turbulence statistics; and 3) compare the predictive capabilities of DES and URANS for a complex internal flow.

NUMERICAL METHOD

The 3D, unsteady, incompressible, Reynolds-averaged Navier-Stokes equations are solved using a dual-time-stepping artificial compressibility iteration scheme. The equations are discretized using a second-order-accurate finite-volume method on a non-staggered computational grid. The convective terms are discretized using the QUICK scheme, and central differencing is employed for the pressure gradients, viscous fluxes and source terms in the turbulence closure equation. The method of Sotiropoulos and Abdallah (1991) is employed to eliminate odd-even decoupling of the pressure field. The discrete equations are integrated in pseudo time using the pressure-based implicit preconditioner of Sotiropoulos and Constantinescu (1997) coupled with V-cycle multigrid and local pseudo time stepping for faster convergence.

A random flow generation (RFG) technique (Smirnov et al., 2001) was employed to generate non-homogeneous, anisotropic, instantaneous inlet conditions. The RFG tech-

nique generates instantaneous and divergence-free velocity fields with prescribed mean flow and Reynolds stresses, which can be obtained either from experimental measurements or from results of steady RANS computations. In this study, the experimental measurements of Kim and Patel (1994) were used. Note that imposing a forcing on the inlet flow was found to be critical prerequisite for exciting and sustaining unstable modes inside the concave wall boundary layer, regardless of the specific turbulence closure model employed. Non-reflecting, characteristic-based boundary conditions were applied at the outlet boundary to allow vortical structures to exit the flow domain without distortion.

For the RANS simulations (both in steady and unsteady modes), we employ the one-equation Spalart-Allmaras (1994) (SA) model and the two-equation low-Re k-ω (Wilcox, 1988) model. These models are referred to as RANS-SA, URANS-SA and URANS-$k\omega$, respectively. For the DES, we employ the standard hybrid LES/URANS-SA model as outlined in Spalart et al. (1997) and Squires et al. (2002).

TEST CASE AND COMPUTATIONAL DETAILS

The test case was studied experimentally by Kim and Patel (1994) who reported detailed mean flow and turbulence statistics measurements for $Re = 2.24 \times 10^5$ based on the duct width (H) and the mean bulk velocity. The cross-section of the duct is rectangular with a 6:1 height-to-width aspect ratio. The computational domain starts 3.5H upstream from the inlet of the bend and extends up to 7.5H downstream from the exit of the bend (see Fig. 1). We discretized the entire duct cross-section (without invoking any symmetry assumptions) using a total of 1.33 million grid nodes ($145 \times 69 \times 133$ nodes in the streamwise, radial and normal directions, respectively). The first grid node off the wall was located at $y^+ = 0.75$ almost everywhere. The computation was initialized with the steady RANS results obtained by Sotiropoulos and Ventikos (1998). At every physical time step, a converged solution in pseudo time was obtained by requiring 2.5 to 3 orders of magnitude reduction of the momentum residuals. This level of reduction typically required 40 sub-iterations.

RESULTS AND DISCUSSION

The mean flow characteristics of this flow have been discussed in great detail in both the experimental work of Kim and Patel (1994) and the numerical work of Sotiropoulos and Ventikos (1998). In this section, we focus our attention on the dynamics of the unsteady coherent vortical structures along the concave wall and their effect on the mean flow and turbulence statistics.

The three-dimensional structure of the flow along the concave wall is illustrated in Figure 2, which shows an instantaneous snapshot of two iso-surfaces of normalized helicity (the cross-product of velocity and vorticity). This figure shows the formation of the pressure-driven streamwise vortices near the inner wall and the formation of streamwise vortical streaks along the outer wall. It is worth noting that the imposed unsteady forcing of the inlet flow has a relatively small effect on the characteristics of the inner wall, pressure-driven vortex structure. The flow in this region is found to be essentially quasi-steady, undergoing very low amplitude temporal oscillations about its steady-state structure. As seen in Figure 2, however, the imposed forcing dramatically alters the structure of the flow along the concave wall giving rise to the observed coherent streamwise vortical structures. The structures appear in pairs of opposite sign vorticity and meander seemingly randomly in space. Their streamwise extent exhibits considerable spatial and temporal variability and is typically of the order of several boundary layer thicknesses.

To better visualize the spatial structure of the simulated structures, we show in Figure 3 contours of the instantaneous fluctuating streamwise velocity component at plane $y/H = 0.05$ away from the concave wall. Dark regions in this figure represent negative fluctuations (less than the mean) while light regions represent positive fluctuations. This figure clearly demonstrates that the outer wall streaks originate approximately halfway through the bend and persist in the downstream straight tangent. Note that even though Figs. 2 and 3 show DES results, very similar unsteady vortical structures emerge inside the concave wall of the duct in all URANS computations as well.

Figures 4 and 5 compare the DES predictions at station D1 (see Fig. 2) with the time-averaged measurements of Kim and Patel (1994) in terms of streamwise velocity and vorticity components. In both figures, we show simulated results at three snapshots in time and the corresponding time-averaged flow field. As discussed above, the unsteady forcing at the inlet has only a small effect on the flow near the inner wall, which at all times remains essentially similar to its steady-state structure and in good overall agreement with the mean measurements of Kim and Patel (1994). The growth of unsteady vortical structures along the outer wall, on the other hand, is evidenced by the mushroom-like structure of the streamwise velocity contours in Fig. 4. The spanwise variation of the velocity field along the outer wall is consistent with the presence of pairs of counter-rotating vortices with common flow away from the wall as shown in Fig. 5. It is important to note that the time-averaged velocity and vorticity fields exhibit essentially no signs of their three-dimensional instantaneous structure. This finding is consistent with the measurements of Kim and Patel (1994) who reported no significant spanwise variations of the mean flow along the concave wall. The fact that the vortical streaks do not contribute to the mean flow points to the conclusion that they meander randomly in space-a feature consistent with the conclusions reached by Barlow and Johnston (1988) concerning the structure of what they referred to as "*roll cells*" in concave wall boundary layers.

Figure 6 compares the power spectra of the streamwise velocity component computed by DES and URANS models at selected points on station D1 (see also Fig. 5 for point locations). A peak in the power spectra is discernable at point b in the center region near the top and bottom walls. Weak unsteady modes in this region are excited due to the interaction of the two counter-rotating vortices (see Fig. 5) that evolved from the contraction induced vortex pair at the duct inlet in the experimental apparatus (see Kim and Patel (1994) for details). In stark contrast to the inner wall, the growth of vortical streaks inside the centrifugally unstable outer wall boundary layer excite unsteady modes whose magnitude of power spectrum is more than one order of magnitude higher. The spectrum distribution is concentrated in the low frequency regime with a dominant frequency and several harmonics. The Strouhal number of the dominant frequency is around 0.05. Although power spectra predicted by DES and the two URANS models show different magnitudes-with the DES in general predicting more intense unsteadiness-it is notable that the predicted frequencies are

almost identical in this region.

Comparisons of radial profiles of the computed mean velocity and turbulence statistics from the DES and all URANS models and the measurements at stations 45 and D1 are shown in Figs. 7-10 at three vertical locations from the bottom wall (z = 0.25, 0.5, 3.0). For reference, predictions using the steady RANS with the Spalart-Allmaras turbulence model are also included in these Figs. 7, 8 and 10. Figure 7 shows the measured and computed time-averaged velocity profiles at station 45. The measured velocity profiles at this cross section are distorted due to the contraction-induced vortex pair. The transverse pressure gradient, on the other hand, gives rise to significant secondary motion that reduces the streamwise velocity near the inner wall. The predictions of streamwise velocity profiles by all closure models are almost identical and are in reasonable agreement with the measurements. DES and URANS predictions of radial velocity are also in good agreement with the measurements, while the RANS model overestimates the radial velocity profiles near the bottom wall. The mean velocity profiles at station D1 are characterized by the distortion of streamwise velocity component by the intense secondary motion, which becomes S-shaped near the inner wall. At this station, the DES predictions are in closest agreement with the measurements, as shown in Fig. 8. The predictions using S-A closure model are closer to the measurements than those by URANS-$k\omega$, especially for the S-shaped distortion of the streamwise velocity near the inner wall and the secondary velocity near the bottom wall. In summary, the DES, URANS, and steady RANS models yield similar results for the mean flow near the outer wall while the unsteady models improve considerably the prediction of the pressure-driven secondary motion near the inner wall vortical region.

Calculated profiles of the resolved turbulence kinetic energy (TKE) at stations 45 and D1 are shown in Fig. 9. It is evident from this figure that the resolved unsteady modes by all models contribute a negligible amount of TKE near the inner wall but are responsible for a significant amount of energy near the outer wall, especially at the D1 section. The distinct spike seen at the center of the cross-section at both stations near the bottom wall is due to unsteady modes excited by the interaction of the contraction induced vortices (see Fig. 5). In our simulations, these vortices are introduced in the inlet conditions (using the experimental data of Kim and Patel 1994), they are well defined features of the mean flow and due to the imposed inlet forcing undergo unsteady fluctuations about their stationary mean location. The spike in the TKE profiles in this region is significant in the DES and URANS-SA predictions but very weak in the URANS-$k\omega$ model. It is important to emphasize the significant structural difference between the simulated spike in the resolved TKE at the center of the cross section near the bottom wall and the dramatic increase of resolved TKE inside the concave wall boundary layer. The former is due to unsteady interaction among vortices that are well defined features of the mean flow while the latter is due to the random, unsteady meandering of coherent structures that have zero mean (see Figs. 4 and 5). The dramatic increase of resolved TKE near the concave wall is visible in both the DES and URANS solutions with the DES predicting consistently higher levels of TKE. Figure 10 compares the measured and predicted Reynolds shear stress $\overline{uv}$ profiles at the duct plane of symmetry at station D1. The steady RANS and all unsteady simulations yield essentially identical shear stress profiles near the inner wall, which is in excellent agreement with the experimental data. Significant discrepancies do exist, however, near the outer wall where the steady RANS grossly underestimates the magnitude of the primary Reynolds stress. Note that the RANS-SA prediction shown in this figure is very similar with the steady RANS prediction reported by Sotiropoulos and Ventikos (1998) using a variety of linear and non-linear turbulence models and reinforces the inability of steady RANS models to predict concave curvature effects. The DES and URANS predictions, on the other hand, not only yield significantly higher Reynolds stress but also predict the peak in the profile to be much closer to the location of the plateau in the experimental data. The results shown in Fig. 10 along with the rich spatiotemporal dynamics of the flow within the concave wall boundary layer essentially verify the conclusion reached by Barlow and Johnston (1988), namely that "*... increases in turbulence intensities and Reynolds stresses across the outer layer are due almost entirely to increased energy in low-frequency, large-scale fluctuations...*"

In spite of the considerable improvement, discrepancies between measured and predicted profiles, however, do remain in Fig. 10. Given the role of the concave wall coherent vortical streaks in producing the dramatic increase in turbulence statistics, however, it is likely that further improvements could be achieved by substantially refined grids and smaller time increments. Such numerical sensitivity studies have not been performed in this work but are currently under way and will be reported in a future communication.

SUMMARY AND CONCLUSIONS

DES and URANS using a pseudo-turbulent instantaneous inflow condition have been carried out to simulate incompressible flow in a strongly curved, 90-degree, rectangular bend. The following conclusions can be drawn from this work.

The imposed inlet forcing has a relatively small effect on the large-scale flow near the inner bend but dramatically alters the structure of the flow inside the centrifugally unstable concave wall boundary layer. Both in the DES and URANS calculations, the outer wall flow loses stability in the form of pairs of low-frequency, counter-rotating streamwise vortical streaks that originate halfway through the bend and span the entire cross section.

The simulated vortical streaks are not well defined, stable vortices but rather meander randomly in space and appear to have zero mean. Their presence does not cause any appreciable spanwise variation of the mean flow but accounts for a considerable amount of the total Reynolds stresses near the outer wall of the bend. Therefore, the picture that emerges from our computations appears to be consistent with the conclusions reached by Barlow and Johnston (1988) regarding the presence of randomly meandering "*roll cells*" instead of coherent streamwise vortices in concave wall turbulent boundary layers.

Statistical turbulence models that directly resolve large-scale organized unsteady structures in the flow should be the entry level models for accurate predictions of concave curvature effects. Both the DES and URANS models were shown to capture and sustain the onset of the centrifugal instability with the DES yielding more intense vortical streaks and overall better agreement with the experimental data. However, appreciable discrepancies between measured and predicted Reynolds-stresses near the concave wall do remain. Future work should focus on grid refinement and time step sensitivity studies.

ACKNOWLEDGMENTS

This work was supported by NSF Career grant 9875691 and a grant from Oak Ridge National Laboratory and DOE.

REFERENCES

Barlow, R. S., and Johnston, J. P., 1988, "Structure of Turbulent Boundary Layers on a Concave Surface," *Journal of Fluid Mechanics*, Vol. 191, pp. 137-176.

Kim, W. J., and Patel, V. C. 1994, "Origin and Decay of Longitudinal Vortices Developing in a Curved Rectangular Duct," *ASME Journal of Fluids Engineering*, Vol. 116, pp. 45-51.

Lund, T. S., and Moin, P., 1996, "Large-Eddy Simulation of a Concave Wall Boundary Layer," *International Journal of Heat and Fluid Flow*, Vol. 17, No. 3, pp. 290-295.

Patel, V. C., and Sotiropoulos, F., 1997, "Longitudinal Curvature Effects in Turbulent Boundary Layers," *Progress in Aerospace Science*, Vol. 33, pp. 1-70.

Smirnov, A., Shi, S., and Celik. I., 2001, "Random Flow Generation Technique for Large Eddy Simulations and Particle Dynamics Modeling," *ASME Journal of Fluids Engineering*, Vol. 123, pp. 359-371.

Sotiropoulos, F., and Abdallah, S., 1992, "A Primitive Variable Method for the Solution of External, 3-D Incom-pressible, Viscous Flows," *Journal of Computational Physics*, Vol. 103, pp. 336-349.

Sotiropoulos, F., and Constantinescu, G., 1997, "Pressure-Based Residual Smoothing Operators for Multistage Pseudo Compressibility Algorithms," Journal of Computational Physics, Vol. 133, pp. 129-145.

Sotiropoulos, F., and Ventikos Y., 1998, "Prediction of Flow through a 90 Bend Using Linear and Non-Linear Two-Equation Models," *AIAA Journal*, Vol. 36, No. 7, pp. 1256-1262.

Squires, K. D., Forsythe, J. R., Morton, S. A., Strang, W. Z., Wurtzler, K. W., Tomaro, R. F., Grismer, M. J., and Spalart, P. R., 2002, "Progress on Detached-Eddy Simulation of Massively Separated Flows," *AIAA Paper 02-1021.*

Spalart, P. R., and Allmaras, S. R., 1994, "A one-equation turbulence model for aerodynamic flows," *La Recherche Aerospatiale*, 1, pp. 5-21.

Spalart, P. R., Jou, W. H., Strelets, M., and Allmaras, S. R., 1997, "Comments on the Feasibility of LES for Wings, and on a Hybrid RANS/LES Approach," *Advances in DNS/LES, 1st AFOSR Int. Conf. on DNS/LES*, Greyden Press, Columbus Oh.

Wilcox, D. C., 1988, "Reassessment of the scale determining equation for advanced turbulence models," *AIAA Journal*, Vol. 26, No. 11, pp. 1299-1310.

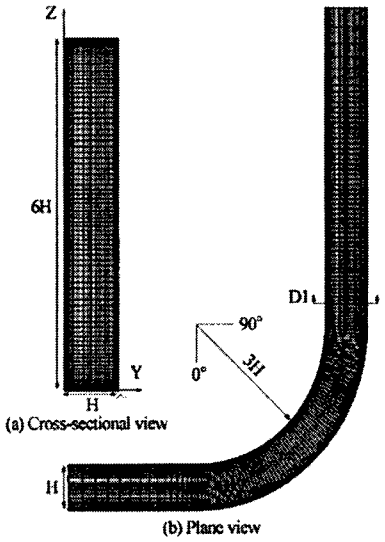

Figure 1: Grid structure and coordinates for the curved duct of Kim and Patel (1994)

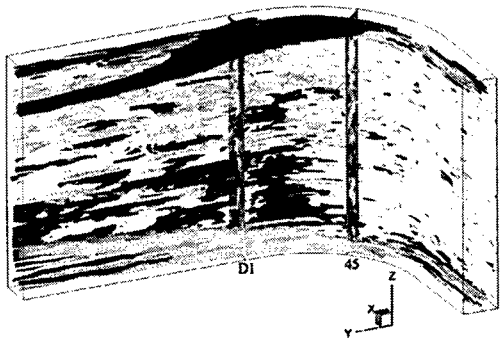

Figure 2: Positive (light) and negative (dark) instantaneous iso-surfaces of normalized helicity (DES)

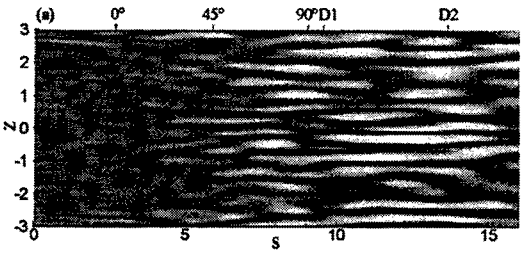

Figure 3: Instantaneous contours of streamwise velocity fluctuations inside the concave wall (DES). Contours range from -0.1 (dark regions) to 0.1 (light regions)

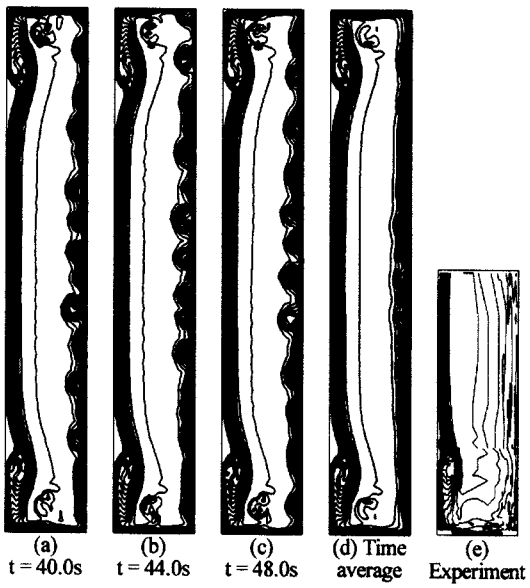

Figure 4: Computed instantaneous (a to c), time-averaged (d), and measured mean contours of streamwise velocity using DES at station D1 (contour levels from 0.6 to 1.1 with an increment of 0.025)

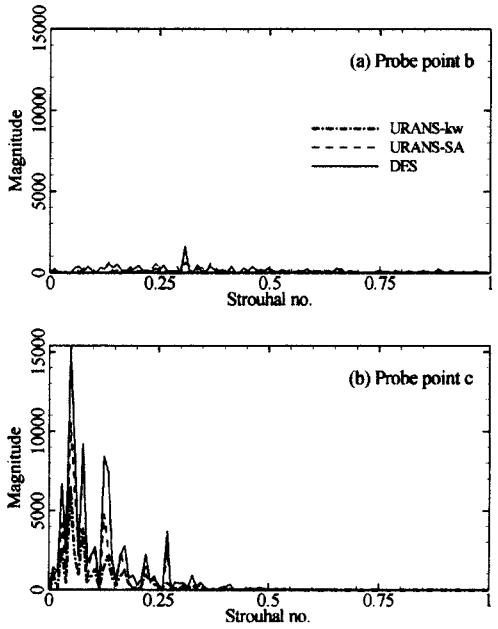

Figure 6: Computed spectra of instantaneous streamwise velocity at station D1 (see Figure 5 for point locations)

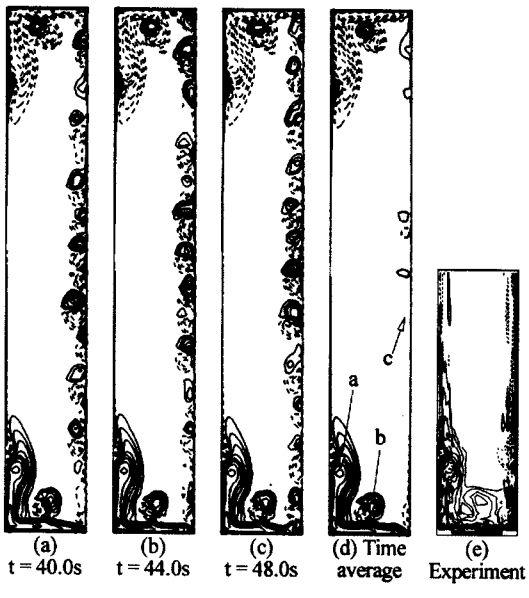

Figure 5: Computed instantaneous (a to c), time-averaged (d), and measured mean contours of streamwise vorticity using DES at station D1. (Ω_x = 0.2, 0.4, 0.6, 0.9, 1.2, 1.5, 2.0 and 2.5)

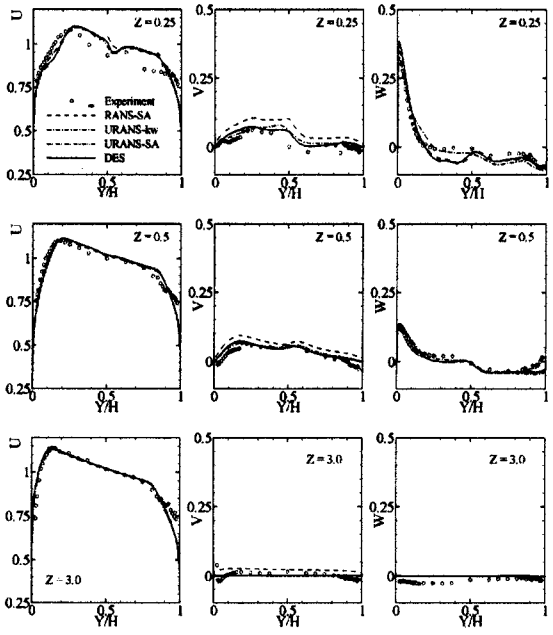

Figure 7: Measured (Kim and Patel 1994) and computed mean streamwise velocity profiles at station 45

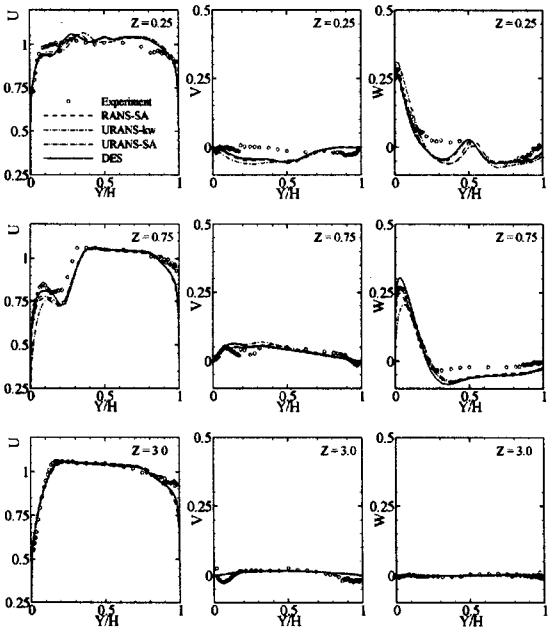

Figure 8: Measured and computed mean streamwise velocity profiles at station D1

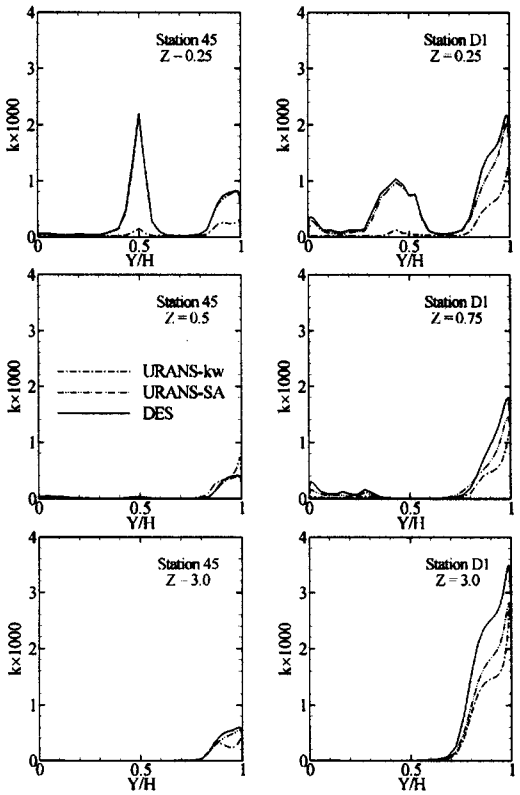

Figure 9: Computed profiles of resolved turbulence kinetic energy at stations 45 and D1

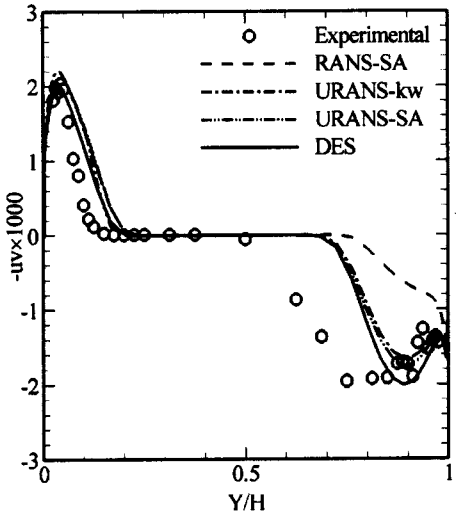

Figure 10: Measured and computed primary shear stress profiles at the plane of symmetry at station D1